How to cite: *Angew. Chem. Int. Ed.* **2022,** *61,* e202114985
International Edition: doi.org/10.1002/anie.202114985
German Edition: doi.org/10.1002/ange.202114985

Polymorphism

Indomethacin Polymorph δ Revealed To Be Two Plastically Bendable Crystal Forms by 3D Electron Diffraction: Correcting a 47-Year-Old Misunderstanding**

Molly Lightowler[+], Shuting Li[+], Xiao Ou, Xiaodong Zou, Ming Lu, and Hongyi Xu**

Abstract: *Indomethacin is a clinically classical non-steroidal anti-inflammatory drug that has been marketed since 1965. The third polymorph, Form δ, was discovered by both melt and solution crystallization in 1974. δ-indomethacin cannot be cultivated as large single crystals suitable for X-ray crystallography and, therefore, its crystal structure has not yet been determined. Here, we report the structure elucidation of δ-indomethacin by 3D electron diffraction and reveal the truth that melt-crystallized and solution-crystallized δ-indomethacin are in fact two polymorphs with different crystal structures. We propose to keep the solution-crystallized polymorph as Form δ and name the melt-crystallized polymorph as Form θ. Intriguingly, both structures display plastic flexibility based on a slippage mechanism, making indomethacin the first drug to have two plastic polymorphs. This discovery and correction of a 47-year-old misunderstanding signify that 3D electron diffraction has become a powerful tool for polymorphic structural studies.*

Introduction

Polymorphism refers to the formation of different crystal packing from a single compound and is an important phenomenon in many areas of science—most notably the pharmaceutical industry.[1,2] Polymorph screening is a necessary step during drug discovery since different polymorphs of the same drug can differ in their physicochemical properties and drug outcomes. Although solution crystallization is the traditional method for polymorph screening, melt crystallization is now revealing a growing list of pharmaceutical polymorphs that cannot be obtained from solution.[3–11] Employing X-ray diffraction techniques is the standard approach for identifying polymorphism and since melt crystallization usually yields polycrystalline spherulites it is challenging to elucidate the structures of melt-crystallized polymorphs. Recently, we developed a general method for rapidly growing single crystals from melt microdroplets.[12] This strategy highly facilitates the structure determination of polymorphs crystallized from the melt.[3,13]

Single-crystal X-ray diffraction (SCXRD), the main workhorse in structural chemistry, requires good-sized crystals (usually larger than 50 μm in each dimension for laboratory diffractometers and 5–10 μm in each dimension for strong synchrotron radiation[14]) of sufficient quality. Many compounds cannot be grown as large crystals and their small crystals often appear to be poor in quality due to a large mosaic spread and/or stacking faults.[15] Therefore, the structure determination of small crystals (very thin plates or very fine needles) is a difficult and long-standing problem.

3D electron diffraction (3D ED) methods, also known as microcrystal electron diffraction (MicroED), have developed rapidly in recent years.[16–20] The ability to solve small molecule structures by 3D ED was first explored using test compounds with known structures (organometallic species[21] and pharmaceutical compounds[14,22–25]) and then compounds with unknown structures (sofosbuvir-L-proline cocrystal,[26] orthocetamol,[27] and loratadine form II[29]). Whilst conceptually 3D ED is comparable to SCXRD, there is a unique advantage to using electrons for diffraction experiments. Thanks to the strong interaction between electrons and matter, 3D electron diffraction data can be collected from very small crystallites. Crystals 10^6 times smaller in volume than those required for X-ray diffraction can now be studied. The power of 3D ED for solving crystal structures of thin organic crystals has been demonstrated using paracetamol and a methylene blue derivative as model compounds.[14] However, good-quality, large crystals of these two compounds can also be grown, meaning the crystals used in the study were also of high-quality despite their small sizes.

Indomethacin (IDM, chemical structure shown in Figure 1) is a clinically classical non-steroidal anti-inflammatory drug discovered in 1963[30] and marketed since 1965. This

[*] M. Lightowler,[+] X. Zou, H. Xu
Department of Materials and Environmental Chemistry
Stockholm University
Stockholm SE-106 91 (Sweden)
E-mail: hongyi.xu@mmk.su.se

S. Li,[+] X. Ou, M. Lu
School of Pharmaceutical Sciences
Sun Yat-sen University
Guangzhou 510006 (China)
E-mail: luming3@mail.sysu.edu.cn

[+] These authors contributed equally to this work.

[**] A previous version of this manuscript has been deposited on a preprint server (https://doi.org/10.33774/chemrxiv-2021-s9fhf).

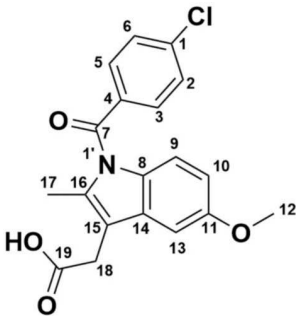

Figure 1. The chemical structure of indomethacin.

drug displays rich polymorphism. In 1968,[31] Yamamoto reported three polymorphs of IDM, α (T_m of 154–155.5 °C), β and γ (T_m of 160–161.5 °C), where T_m refers to the melting point. Form β was later confirmed to be a solvate of IDM by Joshi et al. in 1998.[32] In 1974,[33] Borka reported the third true polymorph of IDM with a T_m of 134 °C, designated as Form III. Borka grew Form III by two methods: spontaneous crystallization from melt between 70–90 °C and from a warm methanol solution. In 1998, Joshi obtained Form III by desolvation of IDM solvates[32] and was the first to report the powder X-ray diffraction (PXRD) data. In 2002, Crowley et al.[34] used Joshi's method to prepare Form III by desolvation of IDM methanolate and renamed this polymorph as Form δ. From this point onwards, people referred to the third polymorph (Form III) of IDM obtained by melt crystallization[35,36] and solution crystallization[37] as Form δ. In 2013, Forms ε, η and ζ were obtained by recrystallization of amorphous IDM in solution under different pH values.[37] The seventh polymorph was discovered in 2018 by recrystallization of IDM from a polyethylene glycol-based solid dispersion.[38] Only the crystal structures of Forms γ ($P\bar{1}$, $Z=2$, Table S1)[39] and α ($P2_1$, $Z=6$, Table S1)[40] are known and were reported in 1972 and 2002, respectively. In this work, we perform microdroplet melt crystallization[12] for single crystal cultivation of δ-IDM crystallized from both melt (melt δ-IDM) and solution (solution δ-IDM) and apply 3D ED for the structure elucidation of both phases.

Results and Discussion

We first grew polycrystalline melt δ-IDM by spontaneous nucleation from supercooled IDM at 60 °C and cultivated single crystals using microdroplet melt crystallization.[12] Single crystals of melt δ-IDM exhibit one-dimensional growth, have a ribbon-like morphology (Figure 2) and are too thin for sufficient X-ray diffraction—even the third-generation synchrotron radiation source.

For 3D ED data collection, single crystals of melt δ-IDM were first separated from the supercooled melt, gently crushed and then loaded onto a holey carbon film supported Cu TEM grid. Data were collected at room temperature using the continuous rotation method.[16–19,41] Since the sample was beam-sensitive, data were collected in small wedges (≈40°) over a large tilt range (−60° to +60°) which

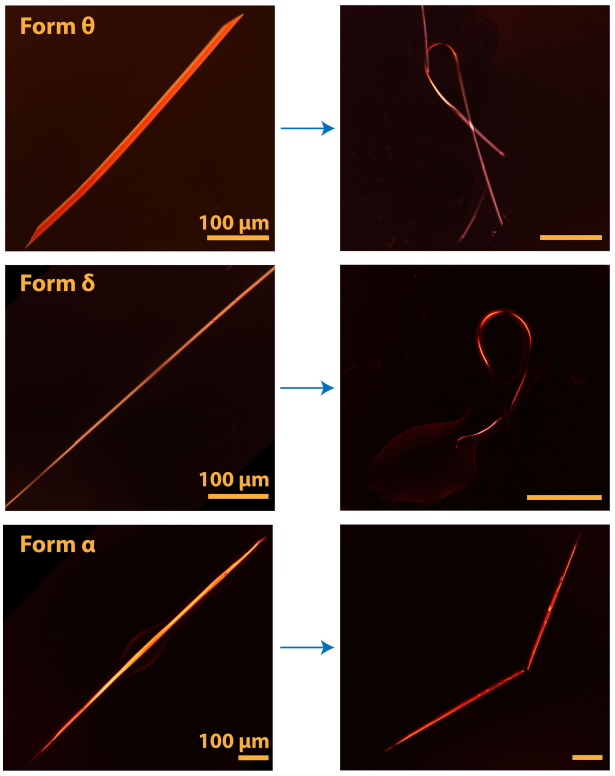

Figure 2. Polarized optical microscopy images of single crystals of IDM polymorphs: Melt δ-IDM (θ-IDM), Solution δ-IDM (δ-IDM) and α-IDM. Left: single crystal before deformation. Right: single crystal after deformation.

helped to achieve sufficient completeness whilst avoiding significant radiation damage. The crushed crystals had a width typically of 0.5–2 µm (Figure S4) and diffracted to a resolution of 1.03 Å. The diffraction frames were indexed using rotation electron diffraction data processing software (REDp)[42] and integrated and merged using XDS.[43] The unit cell parameters were refined against PXRD data using the Pawley method[44] with the TOPAS-Academic v6 program package.[45]

Melt δ-IDM is in the C-centered monoclinic space group *Cc* (No. 9) with the lattice parameters: $a=4.786(1)$ Å, $b=56.999(9)$ Å, $c=12.908(2)$ Å, $\alpha=90°$, $\beta=99.57(1)$ °, $\gamma=90°$ (Figures 3 and S5). Since diffraction data were collected in small wedges, it was necessary to merge individual datasets after indexing to improve completeness and $I/\sigma(I)$ for structure solution and refinement. Seven datasets were chosen for merging based on the similarity of their unit cell dimensions and cross-correlation of indexed intensities (Tables S4 and S5), giving an overall completeness of 70.2 % (Table S3 summarizes the crystallographic information used for the structure solution).

Although the merged data had sufficient resolution (1.03 Å), and $I/\sigma(I)$ (3.7), the structure could not be solved by direct methods. This was likely due to the low completeness (70.2 %) with missing diffraction information around the b^*-axis (Figures 3a and S5, Table S5). The preferred orientation of the crystals on the grid, together with the

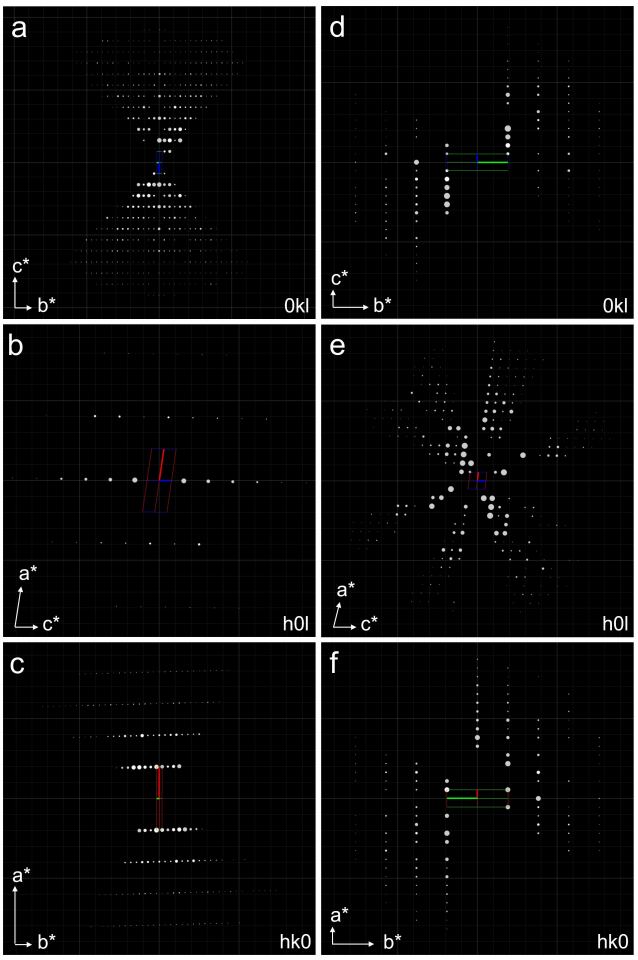

Figure 3. 2D slices of reciprocal lattice planes. a–c) Melt δ-IDM (θ-IDM); the reflection conditions obtained from the 3D ED data show that the crystal space group is *Cc* (No. 9). d–f) Solution δ-IDM (δ-IDM); The reflection conditions show that the crystal space group is $P2_1$ (No. 4).

limited rotation range of the specimen holder, prevented the collection of diffraction information around the *b**-axis. We overcame the problem of missing information by utilizing the simulated annealing method implemented in the program Sir2014[46] as the method for phasing. Woollam et al.[29] demonstrated recently that simulated annealing is a convenient alternative method to reach a structure solution when 3D ED data are not sufficient for structure solution by direct methods. The simulated annealing input requires a molecular model along with the merged ED data. The atom connectivity of γ-IDM (as reported in the CSD, reference code INDMET[39]) was used to create the rigid-body starting fragment in the form of a mol file. According to volume calculations, the asymmetric unit was predicted to contain two crystallographically independent molecules, therefore, two starting fragments were used as the input together with the experimental data. The general conditions for simulated annealing can be found in Table S6. Preliminary structure solutions showed overlapping molecules, this was again due to the lack of diffraction data around the *b**-axis. Anti-bumping restraints were then used to prevent the overlapping. The structure with the lowest cost function (CF = 23.67) was refined by least-squares against the 3D ED data using SHELXL.[47] The final R factor (R1 for all reflections) was 0.1914; the structure is shown in Figure 5 (Table S7 summarizes the experimental crystallographic and refinement data).

Coincidentally, during our study, the structure of solution δ-IDM was solved independently by Andrusenko et. al..[48] We noticed that our two structures of melt δ-IDM and solution δ-IDM were undoubtedly different. This finding led us to ask, do the two crystallization methods that have been thought to produce the same polymorph of IDM since its discovery 47-years ago, Form δ, in fact, produce two different polymorphs?

To carry out further characterization, we grew polycrystalline solution δ-IDM from a pH 6.8 phosphate-buffered saline by partial recrystallization of amorphous IDM and then seeded it in supercooled IDM at 100 °C for growth. PXRD patterns of melt and solution δ-IDM matched the reported data well and are noticeably different when compared to one another (Figures 4a and S1).[32,34–37] Differential scanning calorimetry (DSC) indicated that melt and solution δ-IDM samples exhibit different melting enthalpies, ΔH_m, (26.53 ± 0.69 kJ mol^{-1} for melt δ-IDM and 30.78 ± 0.38 kJ mol^{-1} for solution δ-IDM, $n = 3$) and their Fourier transform Raman and infrared spectra are also contrasting (Figures 4b–d, S2 and S3). The two phases have very similar melting points (134.17 ± 0.76 °C for melt δ-IDM and 133.57 ± 0.29 °C for solution δ-IDM, peak temperature, $n = 3$, Table S2), which may be the reason why they have been mistaken for the same polymorph for almost five decades.

To unambiguously confirm the two phases, we needed to determine the crystal structure of solution δ-IDM. Microdroplet melt crystallization was utilized once more to grow single crystals of solution δ-IDM.[12] The crystals have a needle-like morphology (Figure 2) and, again, display one-

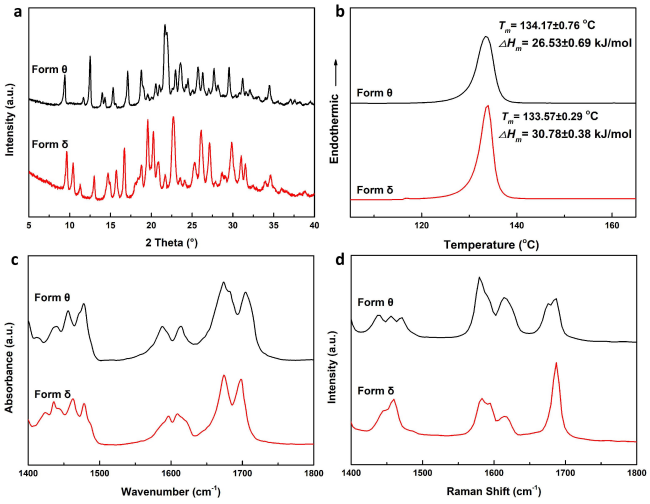

Figure 4. Characterization of melt δ-IDM (θ-IDM) and solution δ-IDM (δ-IDM). a) PXRD patterns; b) DSC curves ($n = 3$); c) Fourier transform infrared spectra; d) Fourier transform Raman spectra.

dimensional growth and are too thin for sufficient X-ray diffraction. The small size of the single crystals may be the reason why the two structures have remained unknown for such a long time.

3D ED data of solution δ-IDM were collected following the same procedure as melt δ-IDM. The crushed crystals had a width typically of 0.5–2.5 μm (Figure S4) and diffracted to a resolution of 1.15 Å. Solution δ-IDM is in the monoclinic space group $P2_1$ (No.4) with the unit cell parameters: $a=18.301(5)$ Å, $b=5.123(1)$ Å, $c=18.564(6)$ Å, $\alpha=90$ °, $\beta=95.80(1)$ °, $\gamma=90$° (Figures 3 and S6). Five datasets were chosen for merging and the overall completeness was 75.0 % (Table S8 summarizes the crystallographic information used for the structure solution). The structure was solved using the simulated annealing method implemented in the program Sir2014,[46] using the same general conditions as melt δ-IDM (Table S6). The structure with the lowest cost function (CF = 29.20) was refined by least-squares against the 3D ED data using SHELXL.[47] The final R factor was 0.1724; the structure is shown in Figure 5 (Table S9 summarizes the experimental crystallographic and refinement data). The simulated and experimental PXRD patterns for both melt and solution δ-IDM correlate well (Figures S7 and S8), confirming the correct structure elucidation and homogeneity for both phases. Our structure of solution δ-IDM is consistent with the structure solved independently by Andrusenko et. al.[48] (Figure S9), further confirming the correct structure elucidation.

Considering that the two structures have now been identified and the two polymorphs distinguished, we propose to keep solution δ-IDM as Form δ (δ-IDM) and name melt δ-IDM as the 8th polymorph of IDM, Form θ (θ-IDM).

The structure of θ-IDM exhibited an extremely long *b*-axis (12 times the *a*-axis and 4.5 times the *c*-axis). By comparing the crystal orientations in real-space images with the corresponding indexed diffraction patterns (Figure S10), the longest crystal dimension was determined to be along the *a*-axis while the shortest dimension is along the *b*-axis. This phenomenon matches the well-observed rule that the fastest growth of crystal occurs along the shortest crystallographic axis.[49,50] The huge difference in size between the *b*-axis and the other axes may be one of the essential reasons for the one-dimensional growth and resulting thin morphology of θ-IDM. The crystal growth direction of δ-IDM was also confirmed to be along the shortest crystallographic axis (Figure S11), however, despite a smaller difference in size of the three crystal axes δ-IDM has a much finer morphology than θ-IDM.

For both θ- and δ-IDM, the asymmetric unit contained two crystallographically independent molecules with very similar conformations, between which a carboxylic acid dimer forms (Figure 5). This dimer also exists in α- and γ-IDM. The dihedral angle in θ-IDM is 25.04°, higher than that in δ-IDM (15.11°), α-IDM (11.76°)[40] and γ-IDM (0°).[39] As shown in Table S10, the eight conformations found in the four IDM polymorphs can be classified into two families based on the torsion angles of θ(C4-C7-N1′-C16): molecule 1 in γ-IDM (151.09°) and molecules 1 and 2 in α-IDM (154.54° and 153.64°) and θ-IDM (159.85° and 152.90°) belong to the same conformational family, while molecule 3 in α-IDM (22.74°) and molecules 1 and 2 in δ-IDM (26.26° and 27.58°) belong to another group.

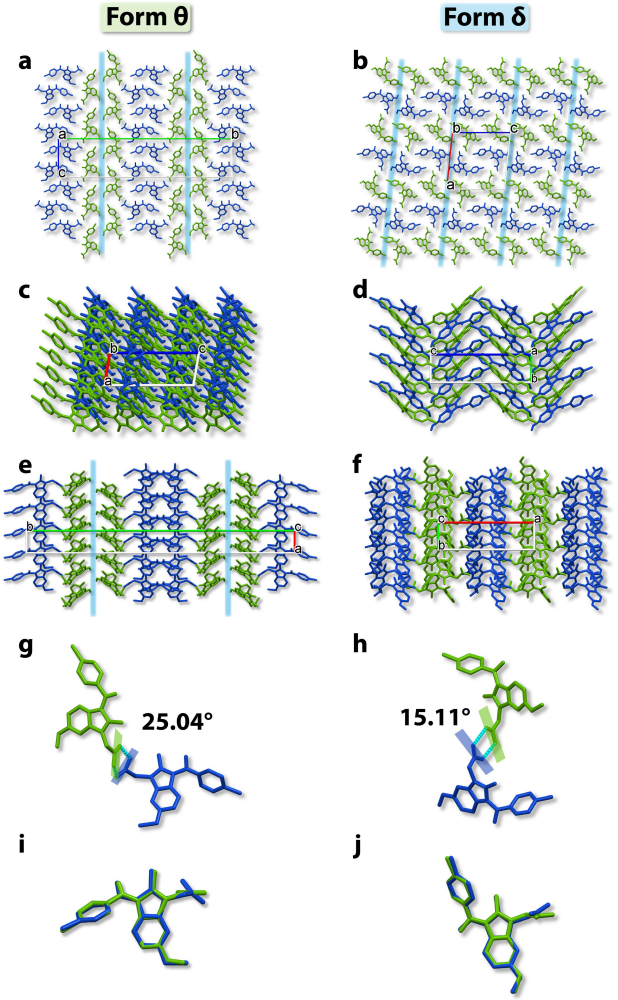

Figure 5. Crystal structures of melt δ-IDM (θ-IDM) and solution δ-IDM (δ-IDM), slip planes are shown in blue. a, d) Molecular packing viewed along the *a*-axis. b, c) Viewed along the *b*-axis. e, f) Viewed along the *c*-axis. g, h) Carboxylic acid dimer formed between the two crystallographically independent molecules and their dihedral angles (blue: molecule 1; green: molecule 2). i, j) Overlay of the two crystallographically independent molecules.

Interestingly, both the ribbon-like θ-IDM and needle-like δ-IDM can undergo one-dimensional plastic deformation in the melt at 120 °C, while needle-like α-IDM is brittle and easy to break under the same conditions (Figure 2). Since single crystals of γ-IDM have a block shape, it was not included in this discussion. θ-IDM single crystals are readily bent down the main face (020) (i.e. *ac* plane, perpendicular to the longest crystal axis, *b*-axis) into the desired shape. After the force is removed, the crystals retain their bent shape. The original shape can be almost recovered with further application of external force. However, if the force is applied to the narrow side of the ribbon (along the shortest axis in geometry), it can easily break, indicative of one-dimensional plastic deformation for θ-IDM. δ-IDM exhibits

similar plasticity. It is difficult to distinguish the main faces (001) and (100) of δ-IDM, which are perpendicular to the shortest crystal axis (*b*-axis) because these needle-like crystals are extremely fine. In our experiments, some δ-IDM single crystals are very brittle and others are plastically bendable. Therefore, we speculate that this difference in mechanical deformation originates from the external force exerted on different crystal faces and plastic deformation of δ-IDM is also one-dimensional.

In θ-IDM, each crystallographically independent molecule packs along the *a*-axis to form π-π stacking between the indole and chlorobenzene rings. Each blue molecule forms a carboxylic acid dimer (2.490 Å, 2.868 Å, 25.04°) with the neighboring green molecule and the two molecules are nearly perpendicular. These right-angle dimers interlock along the *c*-axis to form zippers. Different zipper columns are linked by weak van der Waals interactions, which facilitates the slipping between columns under stress. These slip planes are perpendicular to the *b*-axis (the shortest crystal axis) and parallel to the major face (020) (shown in Figures 5 and 6). In δ-IDM, each molecule in the asymmetric unit packs along the *b*-axis, forming π–π stacking between the indole and chlorobenzene rings. The two crystallographically independent molecules form Z-shaped carboxylic acid dimers (2.859 Å, 2.684 Å, 15.11°) with each other, which are arranged in rows along the *a*-axis (shown in Figures 5 and 6). Weak van der Waals interactions between rows contribute to the formation of slip planes parallel to the face (001). Both θ- and δ-IDM have π-π stacking columns along the shortest crystal axis (*a*-axis for θ-IDM and *b*-axis for δ-IDM) and the slip planes form between molecular columns, while the slip planes cannot be found in brittle α-IDM (Figure 2). Therefore, the slippage of molecular layers along the slip plane is proposed to be the mechanism of plastic deformation of θ- and δ-IDM during bending (see schematic diagram in Figure 6). The layer slippage enables the deformation to occur and the weak interactions between the layers make the deformation irreversible. This slippage mechanism is the most common mechanism of plastic bending for molecular crystals.[51–56] No slip planes can be observed along the b-axis of θ-IDM or the c-axis of δ-IDM. This explains the one-dimensional plastic flexibility of the two polymorphs well.

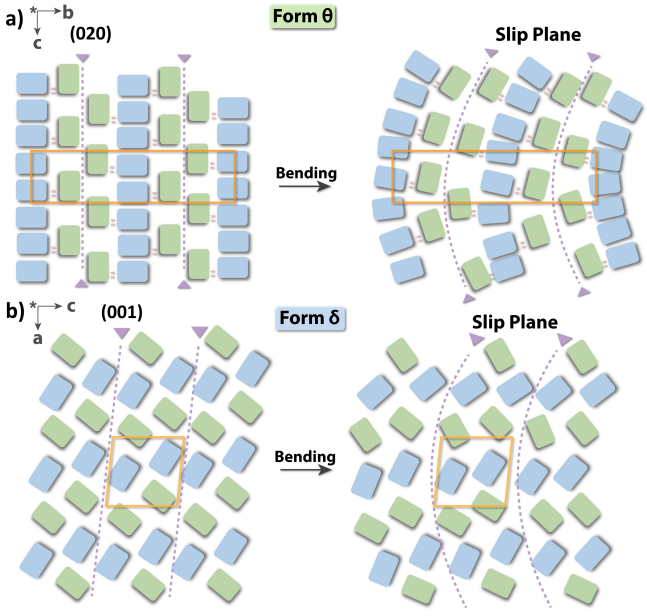

Figure 6. Schematic diagram of bending deformation of IDM polymorphs. a) Melt δ-IDM (θ-IDM). b) Solution δ-IDM (δ-IDM).

Most organic molecular crystals are typically fragile and brittle under excessive stress and plasticity is rare. One compound displaying multiple plastic polymorphs is particularly remarkable. To the best of our knowledge, IDM is the first clinical drug with two phase-pure polymorphs displaying plasticity. Polymorphism that showcases various mechanical behaviors helps us to understand the relationship between crystal structure and solid-state properties[57–60] and also offers an excellent opportunity to tune or predict pharmaceutical-related mechanical properties.[61] For example, the compressibility of an active pharmaceutical ingredient plays an important role in the tabletability of the formulation, especially for high drug-load formulations.[62] Plastic flexibility is advantageous for the tabletability due to the possibility of irreversible plastic deformation via the slippage of molecular layers and resulting improved ability to accommodate stress.[54]

Therefore, the tabletability of θ- and δ-IDM deserves further exploration due to their excellent plasticity compared to other polymorphs, for a better understanding of the relationship between pharmaceutical-related mechanical properties and crystal structure and tuning of the tabletability through crystal engineering. Most plastically bendable molecular crystals were reported at room temperature, while only limited systems were studied above or below room temperature.[63] Since both θ- and δ-IDM exhibit plastic flexibility at a high temperature (120 °C), the dependence of mechanical properties of IDM polymorphs on temperature is also worthy of further investigation.

Conclusion

Through combining microdroplet melt crystallization for single crystal growth with 3D ED for structure determination, we reported that the well-studied δ-IDM samples crystallized from melt and solution are two phases with very similar T_m but different crystal structures. For 47 years, the two crystallization methods were believed to produce the same polymorph. This misunderstanding has been corrected through the fortunate unlikelihood of two independent groups simultaneously solving the respective structures. We proposed to keep the solution-crystallized polymorph as Form δ and name the melt-crystallized polymorph as Form θ. Single crystals of both θ- and δ-IDM are extremely thin, meaning the structures could not be determined by X-ray crystallography—even the third-generation synchrotron radiation. By finally achieving structure determination by 3D ED, the first case of a clinical drug displaying two phase-pure polymorphs with plastically bendable properties was

revealed and the potential to tune the mechanical properties of drugs by polymorph selection was suggested. The successful single crystal growth and structure elucidation of both phases highlight the advancements in crystallization technology and emphasize the importance of 3D ED in polymorphic discovery and structural studies, especially for cases of very thin crystals that are beyond the capability of X-ray crystallography. We are confident that in the future, when 3D ED is more established and available to a wider field of researchers, further misunderstandings will be corrected and more mysteries will be solved.

Acknowledgements

We are grateful to A. K. Inge, Stockholm University, for his expertise and support regarding the work relating to X-ray diffraction and to Prof. Bin Tian (Shaanxi University of Science and Technology, China) and Prof. Lian Yu (University of Wisconsin-Madison, USA) for their helpful discussions regarding indomethacin polymorph δ. We acknowledge funding of the Swedish Research Council (2017-05333, 2019-00815), the Knut and Alice Wallenberg Foundation (2019.0124), SciLifeLab technology development project (MicroED@SciLifeLab) and Guangdong Basic and Applied Basic Research Foundation (No. 2020A1515010782).

Conflict of Interest

The authors declare no conflict of interest.

Data Availability Statement

The data that support the findings of this study are openly available in https://zenodo.org/ at After publishing, reference number 0.

Keywords: Electron Diffraction · Indomethacin · Melt Crystallization · Plasticity · Structure Elucidation · Polymorphism

[1] A. J. Cruz-Cabeza, S. M. Reutzel-Edens, J. Bernstein, *Chem. Soc. Rev.* **2015**, *44*, 8619–8635.
[2] D. K. Bučar, R. W. Lancaster, J. Bernstein, *Angew. Chem. Int. Ed.* **2015**, *54*, 6972–6993; *Angew. Chem.* **2015**, *127*, 7076–7098.
[3] X. Li, X. Ou, B. Wang, H. Rong, B. Wang, C. Chang, B. Shi, L. Yu, M. Lu, *Commun. Chem.* **2020**, *3*, 152–160.
[4] Y. Gui, X. Yao, I. A. Guzei, M. M. Aristov, J. Yu, L. Yu, *Chem. Mater.* **2020**, *32*, 7754–7765.
[5] K. Zhang, N. Fellah, A. G. Shtukenberg, X. Fu, C. Hu, M. D. Ward, *CrystEngComm* **2020**, *22*, 2705–2708.
[6] D. Skomski, R. J. Varsolona, Y. Su, J. Zhang, R. Teller, S. P. Forster, S. E. Barrett, W. Xu, *Mol. Pharm.* **2020**, *17*, 2874–2881.
[7] A. G. Shtukenberg, M. Tan, L. Vogt-Maranto, E. J. Chan, W. Xu, J. Yang, M. E. Tuckerman, C. T. Hu, B. Kahr, *Cryst. Growth Des.* **2019**, *19*, 4070–4080.
[8] M. A. Ciciliati, M. E. S. Eusébio, M. R. Silva, É. T. G. Cavalheiro, R. A. E. Castro, *CrystEngComm* **2019**, *21*, 4319–4328.
[9] Q. Zhu, A. G. Shtukenberg, D. J. Carter, T. Q. Yu, J. Yang, M. Chen, P. Raiteri, A. R. Oganov, B. Pokroy, I. Polishchuk, P. J. Bygrave, G. M. Day, A. L. Rohl, M. E. Tuckerman, B. Kahr, *J. Am. Chem. Soc.* **2016**, *138*, 4881–4889.
[10] C. Yao, I. A. Guzei, Y. Jin, S. Ruan, G. Sun, Y. Gui, L. Wang, L. Yu, *Cryst. Growth Des.* **2020**, *20*, 7874–7881.
[11] N. Fellah, A. G. Shtukenberg, E. J. Chan, L. Vogt-Maranto, W. Xu, C. Li, M. E. Tuckerman, B. Kahr, M. D. Ward, *Cryst. Growth Des.* **2020**, *20*, 2670–2682.
[12] X. Ou, X. Li, H. Rong, L. Yu, M. Lu, *Chem. Commun.* **2020**, *56*, 9950–9953.
[13] X. Li, X. Ou, H. Rong, S. Huang, J. Nyman, L. Yu, M. Lu, *Cryst. Growth Des.* **2020**, *20*, 7093–7097.
[14] T. Gruene, J. T. C. Wennmacher, C. Zaubitzer, J. J. Holstein, J. Heidler, A. Fecteau-Lefebvre, S. De Carlo, E. Müller, K. N. Goldie, I. Regeni, T. Li, G. Santiso-Quinones, G. Steinfeld, S. Handschin, E. van Genderen, J. A. van Bokhoven, G. H. Clever, R. Pantelic, *Angew. Chem. Int. Ed.* **2018**, *57*, 16313–16317; *Angew. Chem.* **2018**, *130*, 16551–16555.
[15] M. M. Harding, *J. Synchrotron Radiat.* **1996**, *3*, 250–259.
[16] I. Nederlof, E. Van Genderen, Y. W. Li, J. P. Abrahams, *Acta Crystallogr. Sect. D* **2013**, *69*, 1223–1230.
[17] M. Gemmi, M. G. I. La Placa, A. S. Galanis, E. F. Rauch, S. Nicolopoulos, *J. Appl. Crystallogr.* **2015**, *48*, 718–727.
[18] B. L. Nannenga, D. Shi, A. G. W. Leslie, T. Gonen, *Nat. Methods* **2014**, *11*, 927–930.
[19] Y. Wang, S. Takki, O. Cheung, H. Xu, W. Wan, L. Öhrström, A. K. Inge, *Chem. Commun.* **2017**, *53*, 7018–7021.
[20] M. Gemmi, E. Mugnaioli, T. E. Gorelik, U. Kolb, L. Palatinus, P. Boullay, S. Hovmöller, J. P. Abrahams, *ACS Cent. Sci.* **2019**, *5*, 1315–1329.
[21] C. G. Jones, M. Asay, L. J. Kim, J. F. Kleinsasser, A. Saha, T. J. Fulton, K. R. Berkley, D. Cascio, A. G. Malyutin, M. P. Conley, B. M. Stoltz, V. Lavallo, J. A. Rodríguez, H. M. Nelson, *ACS Cent. Sci.* **2019**, *5*, 1507–1513.
[22] C. G. Jones, M. W. Martynowycz, J. Hattne, T. J. Fulton, B. M. Stoltz, J. A. Rodriguez, H. M. Nelson, T. Gonen, *ACS Cent. Sci.* **2018**, *4*, 1587–1592.
[23] T. E. Gorelik, J. van de Streek, A. F. M. Kilbinger, G. Brunklaus, U. Kolb, *Acta Crystallogr. Sect. B* **2012**, *68*, 171–181.
[24] E. Van Genderen, M. T. B. Clabbers, P. P. Das, A. Stewart, I. Nederlof, K. C. Barentsen, Q. Portillo, N. S. Pannu, S. Nicolopoulos, T. Gruene, J. P. Abrahams, *Acta Crystallogr. Sect. A* **2016**, *72*, 236–242.
[25] P. P. Das, E. Mugnaioli, S. Nicolopoulos, C. Tossi, M. Gemmi, A. Galanis, G. Borodi, M. M. Pop, *Org. Process Res. Dev.* **2018**, *22*, 1365–1372.
[26] P. Brázda, L. Palatinus, M. Babor, *Science* **2019**, *364*, 667–669.
[27] I. Andrusenko, V. Hamilton, E. Mugnaioli, A. Lanza, C. Hall, J. Potticary, S. R. Hall, M. Gemmi, *Angew. Chem. Int. Ed.* **2019**, *58*, 10919–10922; *Angew. Chem.* **2019**, *131*, 11035–11038.
[28] X. Liu, Y. Luo, W. Mao, J. Jiang, H. Xu, L. Han, J. Sun, P. Wu, *Angew. Chem. Int. Ed.* **2020**, *59*, 1166–1170; *Angew. Chem.* **2020**, *132*, 1182–1186.
[29] G. R. Woollam, P. P. Das, E. Mugnaioli, I. Andrusenko, A. S. Galanis, J. Van De Streek, S. Nicolopoulos, M. Gemmi, T. Wagner, *CrystEngComm* **2020**, *22*, 7490–7499.
[30] F. D. Hart, P. L. Boardman, *Br. Med. J.* **1963**, *2*, 965–970.
[31] H. Yamamoto, *Chem. Pharm. Bull.* **1968**, *16*, 17–19.
[32] V. Joshi, Physical Transformations in Solvated Pharmaceuticals, Purdue University (United States), **1998**.
[33] L. Borka, *Acta Pharm. Suec.* **1974**, *11*, 295–303.
[34] K. J. Crowley, G. Zografi, *J. Pharm. Sci.* **2002**, *91*, 492–507.
[35] T. Wu, L. Yu, *J. Phys. Chem. B* **2006**, *110*, 15694–15699.

[36] B. Tian, W. Gao, X. Tao, X. Tang, L. S. Taylor, *Cryst. Growth Des.* **2017**, *17*, 6467–6476.
[37] S. A. Surwase, J. P. Boetker, D. Saville, B. J. Boyd, K. C. Gordon, L. Peltonen, C. J. Strachan, *Mol. Pharm.* **2013**, *10*, 4472–4480.
[38] T. Van Duong, D. Lüdeker, P. J. Van Bockstal, T. De Beer, J. Van Humbeeck, G. Van Den Mooter, *Mol. Pharm.* **2018**, *15*, 1037–1051.
[39] T. J. Kistenmacher, R. E. Marsh, *J. Am. Chem. Soc.* **1972**, *94*, 1340–1345.
[40] X. Chen, K. R. Morris, U. J. Griesser, S. R. Byrn, J. G. Stowell, *J. Am. Chem. Soc.* **2002**, *124*, 15012–15019.
[41] Y. Wang, T. Yang, H. Xu, X. Zou, W. Wan, *J. Appl. Crystallogr.* **2018**, *51*, 1094–1101.
[42] W. Wan, J. Sun, J. Su, S. Hovmöller, X. Zou, *J. Appl. Crystallogr.* **2013**, *46*, 1863–1873.
[43] W. Kabsch, *Acta Crystallogr. Sect. D* **2010**, *66*, 125–132.
[44] G. S. Pawley, *J. Appl. Crystallogr.* **1981**, *14*, 357–361.
[45] A. A. Coelho, TOPAS-Academic V6, Coelho Software, Brisbane (Australia), **2016**.
[46] M. C. Burla, R. Caliandro, B. Carrozzini, G. L. Cascarano, C. Cuocci, C. Giacovazzo, M. Mallamo, A. Mazzone, G. Polidori, *J. Appl. Crystallogr.* **2015**, *48*, 306–309.
[47] G. M. Sheldrick, *Acta Crystallogr. Sect. C* **2015**, *71*, 3–8.
[48] I. Andrusenko, V. Hamilton, A. E. Lanza, C. L. Hall, E. Mugnaioli, J. Potticary, A. Buanz, S. Gaisford, A. M. Piras, Y. Zambito, S. R. Hall, M. Gemmi, *Int. J. Pharm.* **2021**, *608*, 121067.
[49] K. V. Rajendran, D. Jayaraman, R. Jayavel, P. Ramasamy, *J. Cryst. Growth* **2003**, *255*, 361–368.
[50] S. Manivannan, S. Dhanuskodi, *J. Cryst. Growth* **2004**, *262*, 473–478.
[51] A. Hasija, D. Chopra, *CrystEngComm* **2021**, *23*, 5711–5730.
[52] S. Bhandary, A. J. Thompson, J. C. McMurtrie, J. K. Clegg, P. Ghosh, S. R. N. K. Mangalampalli, S. Takamizawa, D. Chopra, *Chem. Commun.* **2020**, *56*, 12841–12844.
[53] A. Mondal, B. Bhattacharya, S. Das, S. Bhunia, R. Chowdhury, S. Dey, C. M. Reddy, *Angew. Chem. Int. Ed.* **2020**, *59*, 10971–10980; *Angew. Chem.* **2020**, *132*, 11064–11073.
[54] S. Hu, M. K. Mishra, C. C. Sun, *Chem. Mater.* **2019**, *31*, 3818–3822.
[55] G. R. Krishna, R. Devarapalli, G. Lal, C. M. Reddy, *J. Am. Chem. Soc.* **2016**, *138*, 13561–13567.
[56] S. Saha, M. K. Mishra, C. M. Reddy, G. R. Desiraju, *Acc. Chem. Res.* **2018**, *51*, 2957–2967.
[57] K. Zhang, C. C. Sun, Y. Liu, C. Wang, P. Shi, J. Xu, S. Wu, J. Gong, *Chem. Mater.* **2021**, *33*, 1053–1060.
[58] M. K. Mishra, C. C. Sun, *Cryst. Growth Des.* **2020**, *20*, 4764–4769.
[59] X. Chu, Z. Lu, B. Tang, B. Liu, K. Ye, H. Zhang, *J. Phys. Chem. Lett.* **2020**, *11*, 5433–5438.
[60] K. B. Raju, S. Ranjan, V. S. Vishnu, M. Bhattacharya, B. Bhattacharya, A. K. Mukhopadhyay, C. M. Reddy, *Cryst. Growth Des.* **2018**, *18*, 3927–3937.
[61] J. A. Yadav, K. S. Khomane, S. R. Modi, B. Ugale, R. N. Yadav, C. M. Nagaraja, N. Kumar, A. K. Bansal, *Mol. Pharm.* **2017**, *14*, 866–874.
[62] T. V. Joshi, A. B. Singaraju, H. S. Shah, K. R. Morris, L. L. Stevens, R. V. Haware, *Cryst. Growth Des.* **2018**, *18*, 5853–5865.
[63] H. Liu, K. Ye, Z. Zhang, H. Zhang, *Angew. Chem. Int. Ed.* **2019**, *58*, 19081–19086; *Angew. Chem.* **2019**, *131*, 19257–19262.

Manuscript received: November 4, 2021
Accepted manuscript online: December 13, 2021
Version of record online: January 5, 2022